Front. Earth Sci. 2024, 18(2): 336–346
https://doi.org/10.1007/s11707-022-1056-4

RESEARCH ARTICLE

# Quantitative evaluation of adsorbed and free water in deep shales: a case study on the Wufeng-Longmaxi Formations from the Luzhou area, southern Sichuan Basin, China

**Shengxian ZHAO[1,2,3], Yongyang LIU[3], Shuangfang LU (✉)[4], Shuaihu LIU[1,2], Wenbiao LI[4], Zhiyan ZHOU[1,2], Yashuo WANG[1,2], Zhaojing SONG (✉)[1,2]**

1 Key Laboratory of Deep Oil and Gas, China University of Petroleum (East China), Qingdao 266580, China
2 School of Geosciences, China University of Petroleum (East China), Qingdao 266580, China
3 Shale Gas Research Institute of PetroChina Southwest Oil & Gasfield Company, Chengdu 610051, China
4 Sanya Offshore Oil & Gas Research Institute, Northeast Petroleum University, Sanya 572025, China



**Abstract** Deep shale gas reservoirs commonly contain connate water, which affects the enrichment and migration of shale gas and has attracted the attention of many scholars. It is significant to quantitatively estimate the amounts of adsorbed and free water in shale matrix pores, considering the different impacts of pore water (adsorbed water and free water) on shale gas. In this paper, pore water in six deep shale samples from the Wufeng-Longmaxi Formations in the Luzhou area, southern Sichuan Basin, China, was quantitatively evaluated by saturation-centrifugation experiments. Further, the impact of shale material composition and microstructure on the pore water occurrence was analyzed. The results show that amounts of adsorbed and free water are respectively 1.7967–9.8218 mg/g (mean 6.4501 mg/g) and 9.5511–19.802 mg/g (mean 13.9541 mg/g) under the experimental conditions (30°C, distilled water). The ratio of adsorbed water to total water is 15.83%–42.61% (mean 30.45%). The amounts of adsorbed and free water are related to the pore microstructure and material compositions of shale. The specific surface area of shale controls the amount of adsorbed water, and the pore volume controls the amount of free water; organic pores developed in shale solid asphalt contribute specific surface area and pore volume, and inorganic pores developed in clay mineral contribute pore volume. Therefore, the pores of shale solid asphalt accumulate the adsorbed water and free water, and the pores of clay minerals mainly accumulate the free water.

Received October 10, 2022; accepted January 29, 2023

E-mails: lushuangfang@upc.edu.cn (Shuangfang LU)
songzhaojing9707@126.com (Zhaojing SONG)

**Keywords** deep shales, pore water, adsorbed amount, free amount

## 1 Introduction

China has abundant shale gas resources. Exploration and development of shale gas has become a hot spot due to its wide distribution, large resources, and long stable production period (Hao et al., 2013; Liang et al., 2014; Zou et al., 2016). In recent years, China's shale gas production has grown rapidly, and remarkable accomplishments have been achieved in several marine shale gas blocks in the southern Sichuan Basin, including the blocks of Fuling, Weiyuan, Changning, Zhaotong and Fushun-Yongchuan, etc. (Guo et al., 2017; Dong et al., 2018; Jin et al., 2018; Jiao, 2019; Yi et al., 2019; Ma et al., 2020). Shale gas reservoirs, one of the unconventional natural gas reservoirs, commonly contain connate water (i.e., pore water), and has a coexisting characteristic of gas and water under *in situ* condition (Ahmad and Haghighi, 2013; Li et al., 2016; Li et al., 2019a). A large amount of connate water is bound in shale pores, with a water saturation of 10%–90%, which affects the accumulation and seepage of adsorbed gas and free gas in shale reservoirs (Cheng et al., 2017; Li et al., 2019b). Field practice shows that shale reservoirs with a higher connate water saturation have a lower gas content and lower single-well production (Fang et al., 2014; Gasparik et al., 2014; Xu et al., 2022).

As the material basis of shale gas production, *in situ* contents of adsorbed and free gases are significantly affected by the connate water in shale reservoirs (Dehghanpour et al., 2013; Gasparik et al., 2014; Xu

et al., 2022). The influence of water content on the adsorption capacity of shale gas is mainly manifested in two aspects: a) water molecules occupy some of the effective gas adsorption sites on the pore surface, reducing the amount of gas adsorption (Chalmers and Bustin, 2007); b) water molecules obstruct some small pore-throats, reducing the gas storage space (Tang et al., 2017). The impact of water on free gas content is mainly to reduce the gas storage space. Previous scholars have reported that the adsorption capacity of methane in argillaceous shale under the condition of equilibrium water is reduced by 65%−90%, and the adsorption capacity in organic-rich shale is reduced by 20%−60% compared with the dry condition (Ross and Marc Bustin, 2009; Gasparik et al., 2014). Moisture has a great negative impact on the contents of adsorbed gas and gases in shales.

The migration process of shale gas is also under the restrictions of pore water (Pan et al., 2010; Yuan et al., 2014). The transport mechanism of adsorbed gas is surface diffusion, which is affected by pressure gradient and gas adsorption concentration (Yuan et al., 2014; Yang et al., 2016). The transport mechanism of free gas is a continuous flow, gas slippage flow, Knudsen diffusion, and is also affected by factors such as effective stress, matrix shrinkage, and gas desorption during the development process (Wu et al., 2016). The surface diffusivity of adsorbed gas will be affected by the existence of adsorbed water in shale, and the extent of the influence is determined by the amount of adsorbed water (Yuan et al., 2014). In the process of free gas migration, the free path of gas molecules is close to the characteristic scale of pores, and nanoscale effects (such as gas slippage, Knudsen diffusion, etc.) are gradually significant (Loucks et al., 2009; Jiang et al., 2020; Sheng et al., 2020; Yang et al., 2020). For water-bearing shale, when the pore water occupies part of the space, the effective migration channel for gas flow becomes narrower. The pore-throat radius and the thickness of the adsorbed water layer, particularly in the situation of low flow rate (Jiang et al., 2020), are in the same order of magnitude, and the adsorbed water becomes the main factor affecting the free gas seepage (Li et al., 2017a; Sang et al., 2018, 2020). The diffusion coefficient of methane in shale water-containing conditions is significantly lower than that in dry conditions, indicating that water molecules hinder the migration of methane in shale (Yuan et al., 2014). Wu et al. (2014) analyzed the gas-water two-phase flow in nano-pores (100 nm) and showed that when the pore water saturation is 20%, the gas-phase flow capacity is reduced by about 10% compared with the dry condition; In the case of 40%, the gas-phase flow capacity is reduced by about 20%. The permeability of gas generally decreases with increasing water saturation (Zhang et al., 2017; Li et al., 2019b; Wang et al., 2019), therefore the pore water of shale has a significant effect on the migration of shale gas.

Water-bearing characteristics of shales are mainly determined by macro parameters such as initial water saturation, irreducible water saturation, and movable water saturation (Yuan et al., 2018; Yang et al., 2021). Considering the different impacts of pore water (adsorbed water and free water) on shale gas in different states, it is significant to quantitatively estimate the amounts of adsorbed and free water in shale matrix pores. Additionally, in recent years there has been a growing amount of interest in deep shale gas with a burial depth of 3500–4500 m (Jiang et al., 2017; Long et al., 2018; Zhang et al., 2022). Pore water in deep shales was quantitatively evaluated in this study. The amounts of adsorbed and free water in saturated shales were obtained based on the saturation-centrifugation experiments. Further, the impact of shale material composition and microstructure on the pore water was analyzed. The research provides a new idea for the quantitative characterization of shale matrix pore water, which is significant to the exploration and extraction of shale gas.

## 2 Experiments and methodologies

### 2.1 Experimental section

#### 2.1.1 Saturation and centrifugation

Six samples, with a range of burial depths of 3978.13−4047.04 m, were obtained from the deep marine shale reservoirs of the Wufeng-Longmaxi Formation at Well LU206. The well is located in the Luzhou block from the southern Sichuan Basin, China (Zhu et al., 2021). First, the core was prepared into a core column with a 2.5 cm diameter. Secondly, each core column was put into a DZF vacuum drying oven and was dried under a vacuum and 110°C environment for at least 24 h to ensure the residual water in the core is completely removed. After taking it out, the mass of the dry core is tested as $m_1$. Thirdly, the dry core was then put into the ZYB-II saturation instrument and then the core was saturated with distilled water. During the saturation process, 10 MPa fluid pressure and −0.1 MPa vacuum pressure were applied to the experimental core for 12 days. Then, the core was taken out and weighed as $m_2$. Next, the saturated water core was put into the GL-21M refrigerated centrifuge to perform a centrifugation test by setting different centrifugal rotation speeds (3000−10000 r/min, interval 1000 r/min) under the experimental condition of 30°C. Centrifugation has a duration of at least 4 h at each centrifugal rotation speed. Then, the mass was recorded as $m_x$ to determine the movable water amount.

The total water amount can be obtained by

$$Q_t = \frac{m_2 - m_1}{m_1} \times 1000, \quad (1)$$

where $Q_t$ is the total water amount in shale, mg/g; $m_1$ is the mass of the dry core, g; $m_2$ is the mass of the saturated core, mg/g.

And movable water amount ($Q_m$, mg/g) under each centrifugation condition can be obtained by

$$Q_m = \frac{m_2 - m_x}{m_1} \times 1000, \quad (2)$$

where $Q_m$ is the movable water amount under a certain centrifugal force, mg/g; $m_x$ is the mass of core after centrifugation balance, g.

#### 2.1.2 other experiments

Petrology, geochemistry, microstructure, and other analysis tests were also carried out to analyze the influencing factors of adsorbed and free water amounts, including total organic carbon (TOC) content test, X-ray diffraction (XRD) whole-rock mineral analysis, low-temperature nitrogen adsorption, and scanning electron microscope analysis.

### 2.2 Evaluation method

The main states of water in the pores of the shale matrix are adsorbed and free, with free water having the potential to flow and adsorbed water keeping a nearly immobile situation (Li et al., 2019a). However, due to the influence of the pore-throat microstructure of shale, not all free water can flow effectively under certain conditions. Under external conditions (such as centrifugal force), some free water can flow, which is movable water; the part of free water that cannot flow is capillary-bound water. With the change in external conditions, capillary-bound water can be converted into movable water. When all capillary-bound water is converted into movable water, the amount of movable water reaches the maximum value and is equal to the amount of free water (Li et al., 2019a).

Theoretically, as long as the centrifugal force is continuously increased, the capillary-bound water will be continuously converted into movable water, to obtain the maximum movable water amount. However, it is unrealistic to convert all capillary-bound water into movable water by infinitely increasing the centrifugal force of the centrifuge under the current experimental condition. Since the amount of free water cannot be directly obtained through experiments, it is extremely important to find the functional relationship between centrifugal force and movable water amount. In this way, the maximum movable water amount, that is free water amount, can be theoretically calculated through a series of centrifugal that can be realized in the laboratory.

The relationship between movable water amount and centrifugal force is as follows (Li et al., 2019a):

$$Q_m = \frac{Q_f \Delta P}{\Delta P + \Delta P_L}, \quad (3)$$

where $Q_f$ is the maximum movable water amount when the centrifugal force reaches infinity, that is, the free water amount, mg/g; $\Delta P$ is the centrifugal pressure difference (that is, the centrifugal force), MPa; $\Delta P_L$ is the median pressure difference, that is the centrifugal force when the movable water volume reaches half of the free water amount, MPa.

To facilitate the analysis of parameters in Eq. (3), the equation can be converted into a linear function of $1/Q_m$ and $1/\Delta P$:

$$\frac{1}{Q_m} = \frac{\Delta P_L}{Q_f} \frac{1}{\Delta P} + \frac{1}{Q_f}. \quad (4)$$

By fitting the experimental data and establishing a linear relationship between $1/Q_m$ and $1/\Delta P$, the free water amount can be obtained.

Further, the amount of adsorbed water is equal to the difference between saturated water amount and free water amount and can be written as

$$Q_a = Q_t - Q_f. \quad (5)$$

According to the amounts of adsorbed water and free water, the adsorption ratio can also be calculated as follows:

$$r_a = \frac{Q_a}{Q_a + Q_f} \times 100, \quad (6)$$

where $r_a$ is the ratio of adsorbed water to total water, %.

## 3 Results and discussion

### 3.1 Adsorbed and free amounts of pore water

The results of the saturation-centrifugation experiment are shown in Fig. 1(a) and Table 1, showing the movable water amount under different centrifugal force conditions. It can be seen that the movable water volume gradually increases with the increase in centrifugal force, but the growth rate can be seen to slow down significantly. Thus, it can be inferred that when the centrifugal force increases to infinity, the movable water amount tends to a constant value, this value is the amount of free water. According to the relationship between the reciprocal of movable water amount and the reciprocal of centrifugal force (Fig. 1(b)) it can be noted that there is a good linear correlation ($R^2 > 0.99$). The linear relationship can be used to estimate the maximum movable water amount, that is, the free water amount. For the studied shales under the experimental conditions (30°C, distilled water), the amount of free water varies from 9.5511 to 19.802 mg/g (mean 13.9541 mg/g).

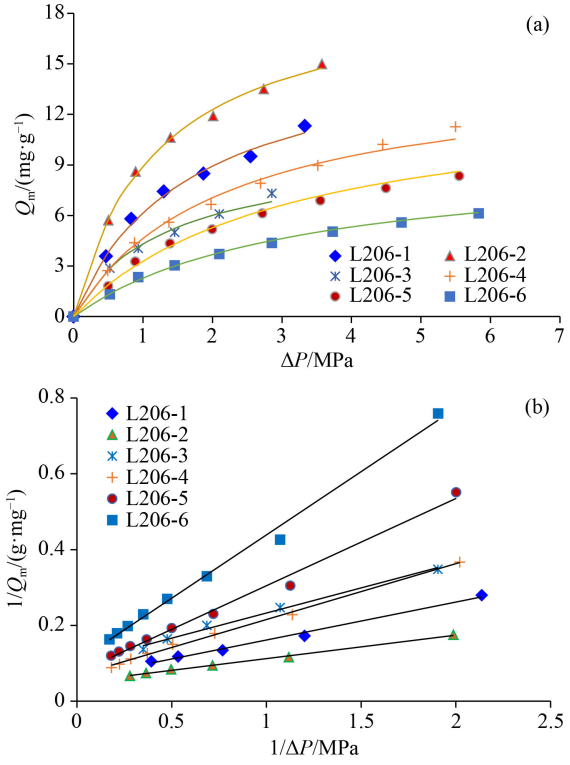


**Fig. 1** Results of centrifugation experiment. (a) Relationship between movable water amount and centrifugal force; (b) relationship between reciprocal of centrifugal force and reciprocal of movable water amount.

Further, the amount of adsorbed water can be calculated by subtracting the amount of free water from the total water amount and varies from 1.7967 to 9.8218 mg/g (mean 6.4501 mg/g). Comparatively, the amount of adsorbed water is larger than free water and accounts for 15.83%–42.61% (mean 30.45%) of total water (Table 2). This demonstrates that part of the water stored in the matrix pores can potentially flow, and will have a certain contribution to the flowback fluid of shale gas well.

Statistics show that the total water amount in shales has a good positive correlation with both adsorbed water and free water amounts (Fig. 2), which implies the coexistence of adsorbed water and free water in the pores of the shale matrix. Vertically, the free water and total water amounts in Well LU206 show an overall trend of decrease, and the change in the amount of adsorbed water is small with the increase in burial depth (Fig. 3). The Wufeng Formation shale has the lowest water-bearing amount and adsorption ratio.

## 3.2 Influencing factors of pore water

### 3.2.1 Coupling relationship between shale compositions and pore microstructure

The occurrence of pore water has an internal relationship with the material composition and pore-throat system (reservoir space) of shale (Hu et al., 2015; Wang et al., 2019; Tian et al., 2020). Various organic/inorganic minerals constitute the rock skeleton, in which a pore-throat system develops, and pore water occurs in the pore-throat. Therefore, in order to reveal the microscopic occurrence mechanism of pore water, it is necessary to clarify the coupling relationship between shale material

**Table 1** Basic information of shale samples

| Sample No. | Burial depth/m | Stratum | Shale constituent content/% | | | | | | | |
|---|---|---|---|---|---|---|---|---|---|---|
| | | | TOC | Q | K | P | C | Fe | Py | Cl |
| L206-1 | 3978.13 | Longmaxi | 2.25 | 34.5 | / | 7.5 | 14.7 | 8.8 | 2.9 | 31.7 |
| L206-2 | 3983.72 | Longmaxi | 3.15 | 43.2 | / | 9.3 | 4.1 | 1.7 | 5.6 | 36.1 |
| L206-3 | 4030.69 | Longmaxi | 3.4 | 39.1 | / | 4.7 | 4.2 | 24.7 | 5.0 | 22.2 |
| L206-4 | 4036.29 | Longmaxi | 4.34 | 61.7 | / | 3.5 | 5.9 | 8.2 | 4.7 | 16.0 |
| L206-5 | 4040.52 | Longmaxi | 3.91 | 53.2 | / | 4.5 | 18.7 | 8.2 | 3.8 | 11.6 |
| L206-6 | 4047.04 | Wufeng | 2.21 | 31.5 | 0.4 | 1.3 | 5.8 | 47.6 | 1.1 | 12.2 |

Notes: Q—Quartz, K—K-feldspar, P—plagioclase, C—Calcite, Fe—ferrodolomite, Py—Pyrite, Cl-Clay minerals.

**Table 2** Calculated results of adsorbed water, free water, and their proportions

| Sample No. | $Q_t$/(mg·g$^{-1}$) | $Q_a$/(mg·g$^{-1}$) | $Q_f$/(mg·g$^{-1}$) | $r_a$/% |
|---|---|---|---|---|
| L206-1 | 21.7286 | 5.3887 | 16.3399 | 24.80 |
| L206-2 | 28.2262 | 8.4242 | 19.802 | 29.85 |
| L206-3 | 17.3546 | 7.3944 | 9.9602 | 42.61 |
| L206-4 | 24.5061 | 9.8218 | 14.6843 | 40.08 |
| L206-5 | 18.9917 | 5.6048 | 13.3869 | 29.51 |
| L206-6 | 11.3478 | 1.7967 | 9.5511 | 15.83 |

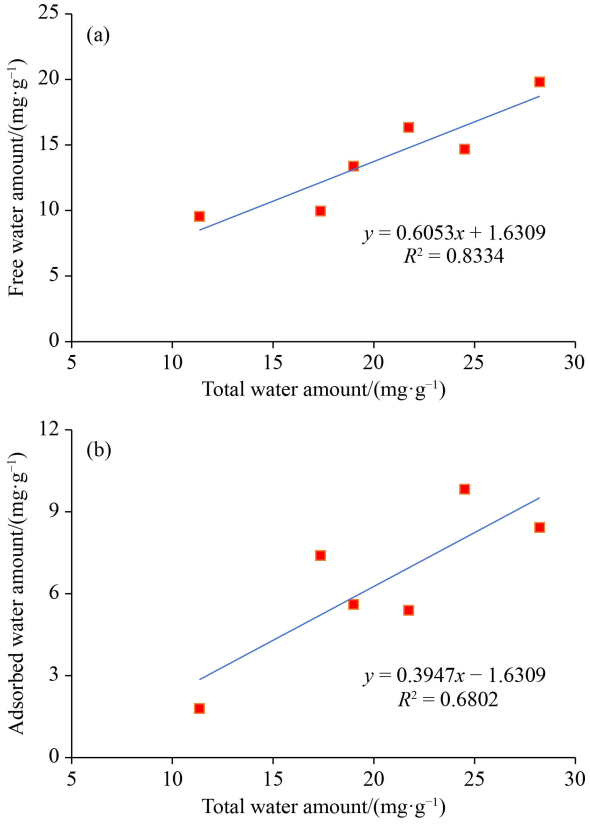


**Fig. 2** Relationships of total water amount with free (a) and adsorbed (b) water amounts.

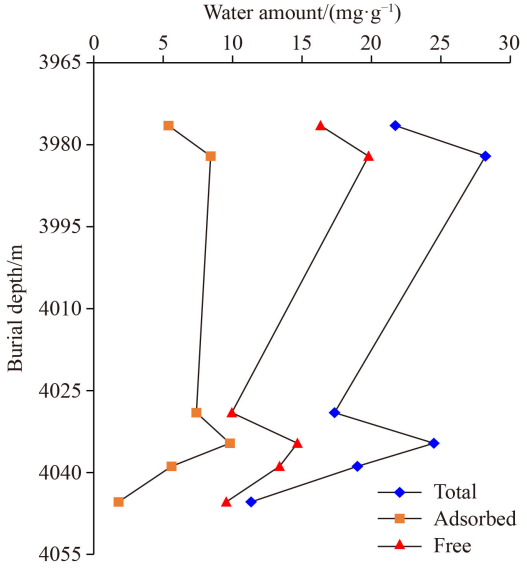


**Fig. 3** Vertical distribution of adsorbed and free water amounts.

composition and pore-throat microstructure.

The inorganic mineral components of the shale in the study area are mainly quartz and clay minerals, accounting for 43.7%–79.3% (mean 65.5%) (Fig. 4(a)). The quartz contents of the shales range from 31.5% to 61.7% (mean 43.9%); the contents of clay minerals range from 11.6% to 36.1%, with an average of 21.6%. Shales develop ferrodolomite (mean 16.5%) and calcite (mean 8.9%) minerals, but the ferrodolomite content in the L206-1 shale sample is abnormally high with a content of 47.6%. In addition, shales contain a small amount of plagioclase and pyrite. Pyrite is an important geochemical indicator mineral, which can indicate the formation environment of organic matter. The pyrite content in the study area is 1.1%–5.6%, with an average of 3.9%. With the increase in burial depth, the content of clay minerals gradually decreased, and the quartz minerals showed a general trend of increase.

Through scanning electron microscope observation, more mineral components can be seen. In addition to the main minerals such as clay, quartz, calcite, ferrodolomite, and pyrite, a small amount of albite, fluorapatite, and titanium dioxide can also be seen (Fig. 5). Crystals of gypsum were even found in localized shale samples. Under the microscope, it can be observed that the intragranular pores of clay particles are generally developed, and some calcites develop intercrystalline pores. In addition, the intercrystalline pores in the gypsum crystals are very developed. However, pores in clay minerals provide major pore space (Fig. 5(a)).

The TOC content of the studied shales is 2.21%–4.34%, with an average of 3.21% (Fig. 4(b)). Through the identification under the microscope, the organic matter of shale is mainly composed of solid bitumen, graptolite, and vitrinite-like, of which solid bitumen is the main organic micro-component, accounting for 48%–80% (mean 64.8%) (Table 3). Graptolite accounts for 15%–46%, with an average of 31.6%. Vertically, the bottom of the Longmaxi Formation of Well LU206 has higher TOC content and solid bitumen ratio, indicating favorable

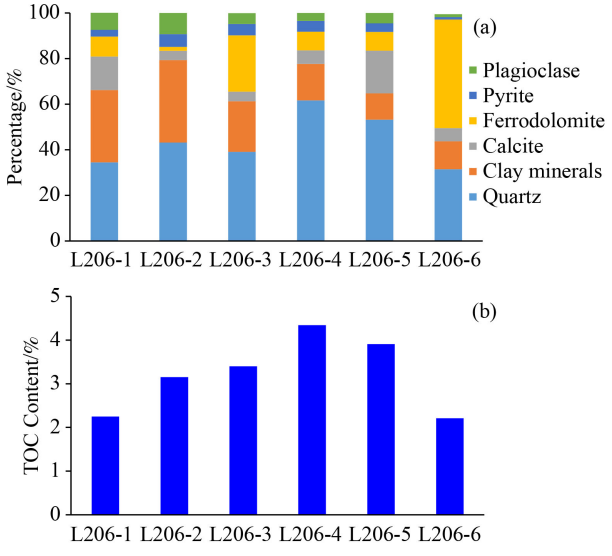


**Fig. 4** Material compositions of studied shales. (a) Inorganic constituents; (b) TOC content.

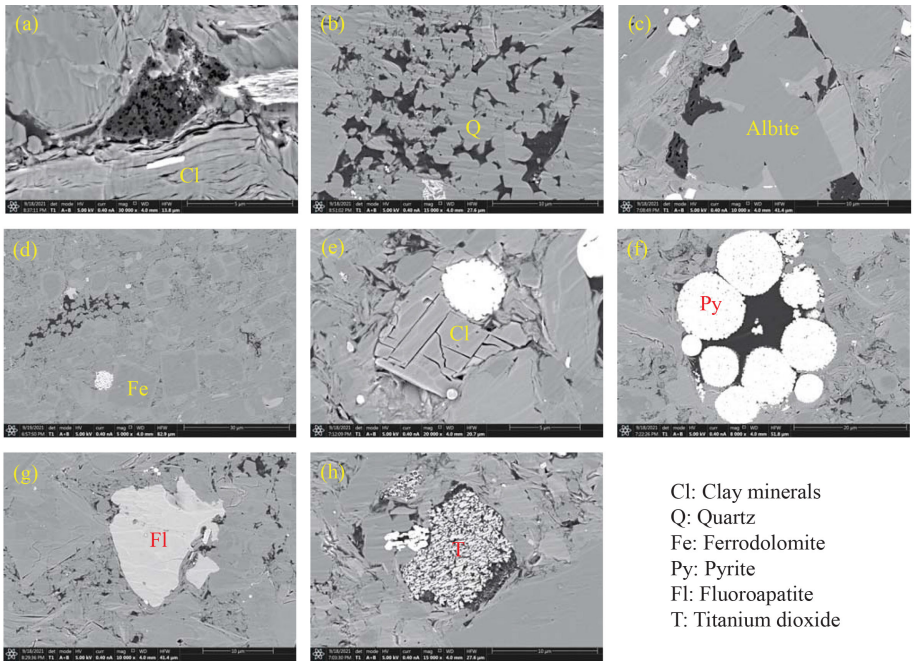


**Fig. 5** Shale inorganic minerals.

exploration and development intervals. Under field emission scanning electron microscope (Fig. 6), the solid bitumen has an irregular shape with clear edges and corners and a large number of nano-pores developed in it. These pores may be the storage space for pore water.

The Luzhou block is located in the center of deep-water continental shelf deposition, and the bottom of the Longmaxi Formation is rich in biosiliceous minerals. The statistical results show that the shale TOC content has a good positive correlation with the quartz mineral content (Fig. 7(a)), showing the characteristics of biogenic silicon, but the pores related to the quartz mineral are not developed (Fig. 5(b)) with a weak contribution to water storage. In addition, there is a certain positive correlation between TOC content and pyrite content (Fig. 7(b)). On the one hand, pyrite indicates a reducing environment, which is conducive to the enrichment of organic matter; on the other hand, pyrite is closely related to hydrocarbon generation (release of sulfur) from organic matter (Berner, 1984; Chen et al., 2021). Thus, organic matter (especially solid bitumen) is usually in a symbiotic state with pyrite (Fig. 5(f)).

**Table 3** Shale organic micro-composition

| Sample No. | Solid bitumen/% | Graptolite/% | Vitrinite-like/% |
|---|---|---|---|
| L206-1 | 48 | 46 | 6 |
| L206-2 | 63 | 32 | 5 |
| L206-3 | 58 | 40 | 2 |
| L206-4 | 72 | 25 | 3 |
| L206-5 | 80 | 15 | 5 |
| L206-6 | 68 | 32 | 0 |

Based on low-temperature nitrogen adsorption/desorption experiments (Li et al., 2017b, 2018), the microstructure of shale was determined, including pore volume, specific surface area, pore size, etc. As shown in Fig. 8, shale pores are dominated by mesopores (2−50 nm), accounting for 73%−78%, with an average of 75%. The statistical results show that the pore volume of shale is positively correlated with the specific surface area (Fig. 9(a)). It may be that the more pores, the higher the pore volume and the specific surface area when the pore size is close. In addition, the higher the proportion of mesopores, the higher the pore volume and the larger the specific surface area (Figs. 9(b)−9(c)).

Finally, the relationship between shale material composition and microstructure is summarized. The positive correlations of TOC and pyrite contents with specific surface area reflect that shale organic pores (mainly developed in solid bitumen) contribute to shale-specific surface area (Figs. 10(a) and 10(b)). Clay and pyrite contents are positively correlated with pore volume (Figs. 10(c) and 10(d)). The correlation reflects that the shale clay mineral intragranular pores and solid bitumen intragranular pores comprehensively contribute to the shale pore volume.

### 3.2.2 Controls of shale compositions and pore microstructure on pore water occurrence

The adsorbed water amount in the pores of the shale matrix is mainly controlled by the specific surface area of shale, and the free water amount is mainly controlled by shale pore volume (Fig. 11). It can also be found that although the amount of adsorbed water is positively

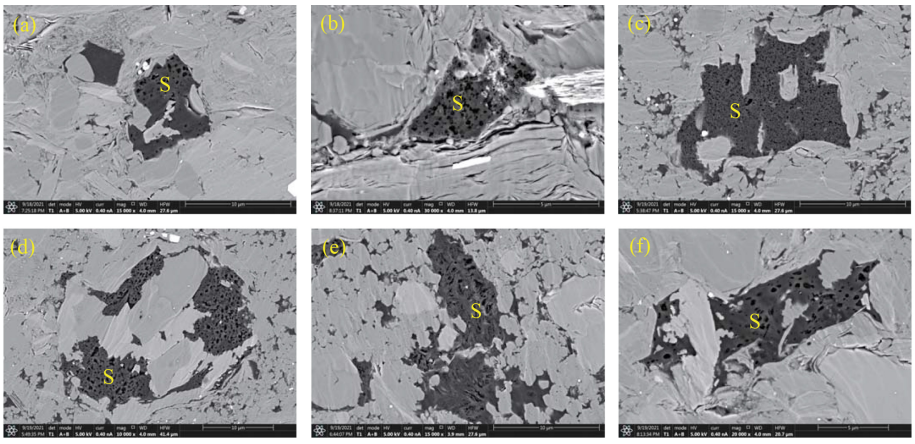


**Fig. 6** Development characteristics of solid bitumen. S is the solid bitumen.

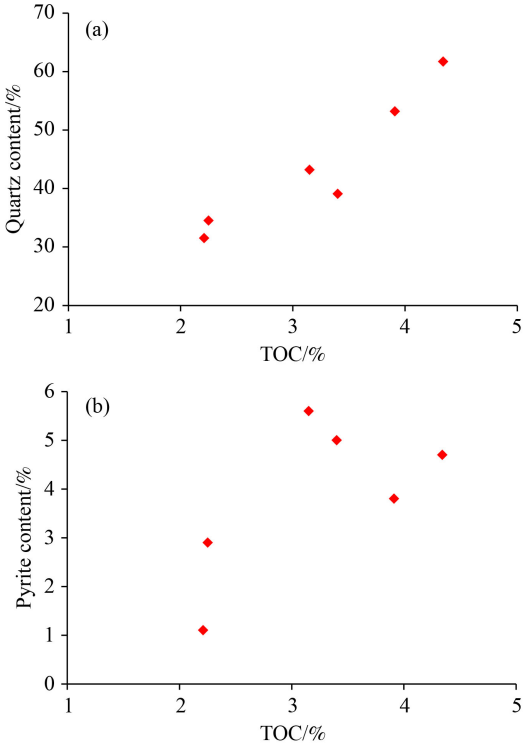


**Fig. 7** Relationships between TOC content and quartz (a) and pyrite (b) contents.

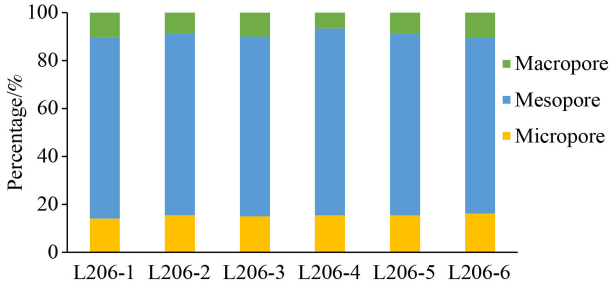


**Fig. 8** The proportion of pores at different scales in shale.

correlated with the specific surface area, and the amount of free water is positively correlated with the pore volume, the regression line has an intercept, indicating that some of the pores determined by low-temperature nitrogen have no adsorbed water or free water. A portion of voids do not contain water. Therefore, it is speculated that there may be a lower limit for the occurrence of pore water in the shale matrix. The adsorbed water in the study area mainly occurs on the pore surface, and the lower limit of the specific surface area is approximately 9 $m^2/g$; the free water mainly occurs inside the pores, and the lower limit of the pore volume is approximately $5 \times 10^{-3}$ $cm^3/g$. After the lower limits of specific surface area and pore volume are determined, the corresponding lower limit values can be subtracted to calculate the specific surface area and pore volume of water-bearing pores in the shale matrix, which lays the foundation for the subsequent evaluation of adsorption parameters. In addition, the lower limit of shale in different regions

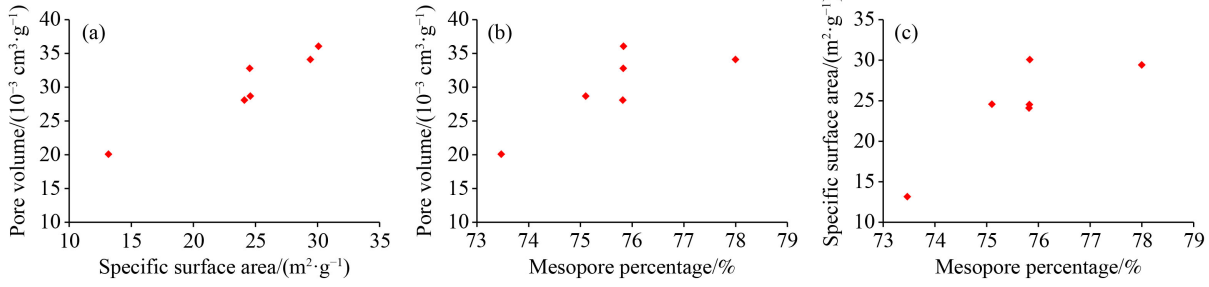


**Fig. 9** Correlation between microstructural parameters.

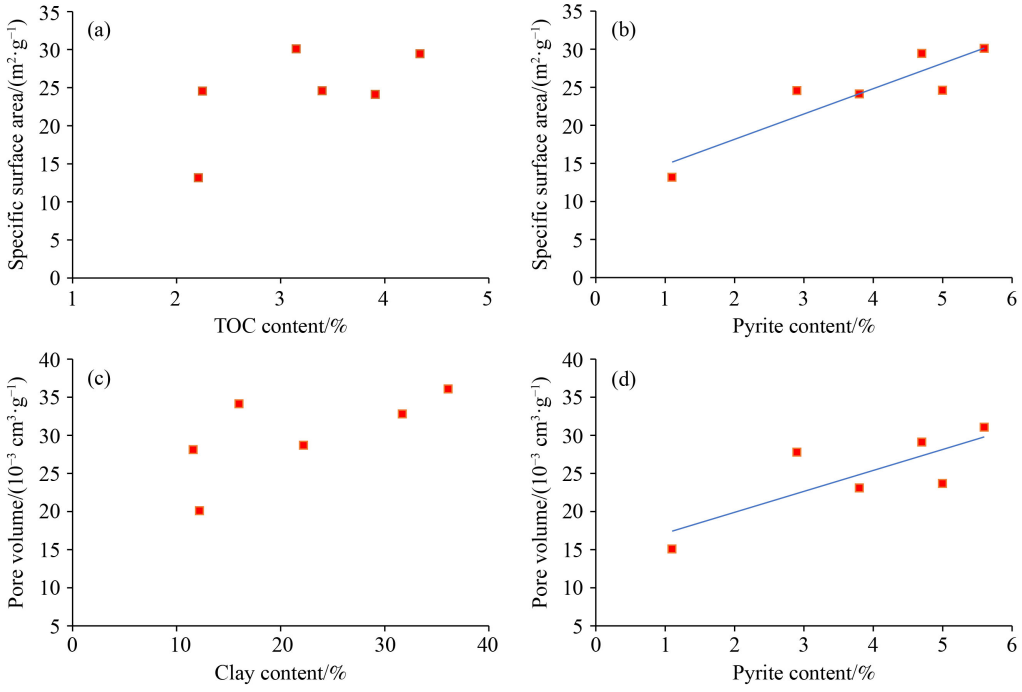


**Fig. 10** The relationship between shale material composition and microstructure.

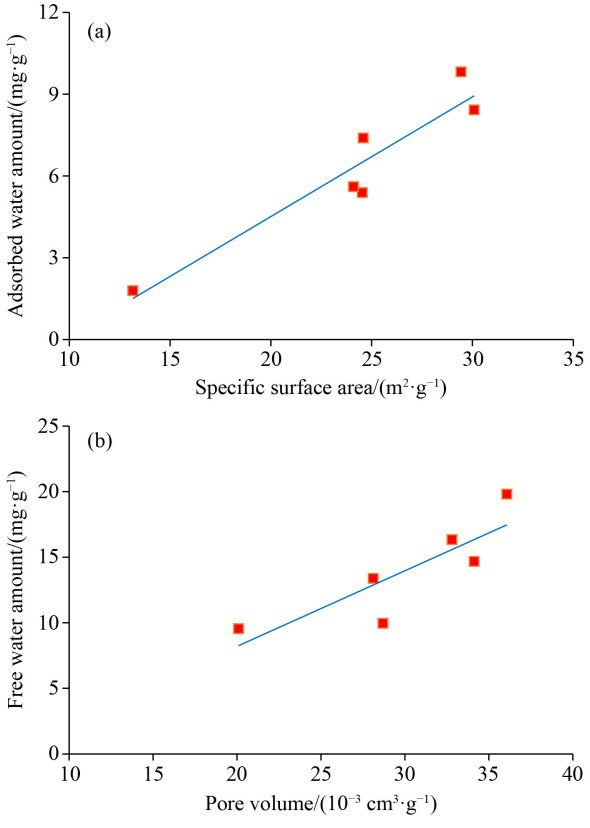


**Fig. 11** Relationship between adsorbed water amount and specific surface area (a), and the relationship between free water amount and pore volume (b).

may be different, which is closely related to the regional depositional environment, shale pore development characteristics, and pore surface properties.

Shale compositions (organic matter and inorganic matter) are complex and the hydrophilic capacity of each component is different (Xie et al., 2015), resulting in significant differences in the water-bearing characteristics of shale organic matter pores and inorganic mineral pores. It is generally believed that the surface of inorganic minerals is usually strongly hydrophilic, especially clay minerals, which have charges on their surfaces, and water molecules and clay particles can be tightly bound by hydrogen bonds, electrostatic forces, and intermolecular forces (Wang and Li, 2006). However, whether there is water in the pores of organic matter is still controversial, and the water may be controlled by factors such as kerogen type, maturity, and functional groups. The organic pores formed during hydrocarbon generation are generally considered to be oil-wet (Odusina et al., 2011), and the pores hardly contain water. However, some studies have shown that the functional group structure in the pores of kerogen makes it exhibit a certain hydrophilic ability, and the water molecules in the pores can be adsorbed on the surface of the functional group (Larsen and Aida, 2004), and distributed in the shale organic matter within pores (Cheng et al., 2017; Li et al., 2019a).

Therefore, the current key geological problem is to clarify in which pore spaces water is stored in shale with different water saturation and reveal the control mechanism of shale material composition and pore-throat system on the occurrence of pore water. The study found that the contents of TOC and pyrite in the well LU206

shales are positively correlated with the amount of adsorbed water; the contents of clay and pyrite are positively correlated with the amount of free water (Fig. 12). This shows that the organic matter (solid bitumen) pores of shale contribute to the amount of adsorbed water and free water, and the pores of clay minerals contribute to the amount of free water.

Finally, the microscopic occurrence mechanism of shale matrix pore water is summarized. The specific surface area of shale controls the amount of adsorbed water, and the pore volume controls the amount of free water; organic pores in shale solid asphalt contribute specific surface area and pore volume, and inorganic pores in clay mineral contribute pore volume. Therefore, the pores of shale solid asphalt contribute to the amount of adsorbed water and free water, and the pores of clay minerals mainly contribute to free water.

## 4 Conclusions

1) This study has shown a quantitative evaluation of pore water in deep shales. As a case study, shale samples were obtained from the Wufeng-Longmax Formations in well LU206, located in the Luzhou area, southern Sichuan Basin, China. The amounts of adsorbed and free water in saturated shales were obtained based on the saturation-centrifugation experiments combined with a new pore water classification scheme proposed by Li et al. (2019a). Under the experimental conditions (30°C, distilled water), the amount of free water varies from 9.5511 to 19.802 mg/g (mean 13.9541 mg/g); the amount of adsorbed water is calculated by subtracting the amount of free water from the total water amount and varies from 1.7967 to 9.8218 mg/g (mean 6.4501 mg/g). The ratio of adsorbed water to total water is 15.83%–42.61% (mean 30.45%).

2) A coupling relationship between shale compositions and pore microstructure was established. The positive correlations of TOC and pyrite contents with specific surface area reflect that shale organic pores (mainly developed in solid bitumen) contribute to shale-specific surface area. Clay and pyrite contents are positively correlated with pore volume reflecting that the shale clay mineral intragranular pores and solid bitumen intragranular pores comprehensively contribute to the shale pore volume.

3) The impact of shale material composition and microstructure on the pore water was analyzed. Based on this, the microscopic occurrence mechanism of shale matrix pore water is revealed. The specific surface area of shale controls the amount of adsorbed water, and the pore volume controls the amount of free water. The pores of shale solid asphalt contribute to the amount of adsorbed water and free water, and the pores of clay minerals mainly contribute to free water.

**Acknowledgments** This work was supported by the National Natural Science Foundation of China (Grant No. 41972123).

**Competing interests** The authors declare that they have no competing interests.

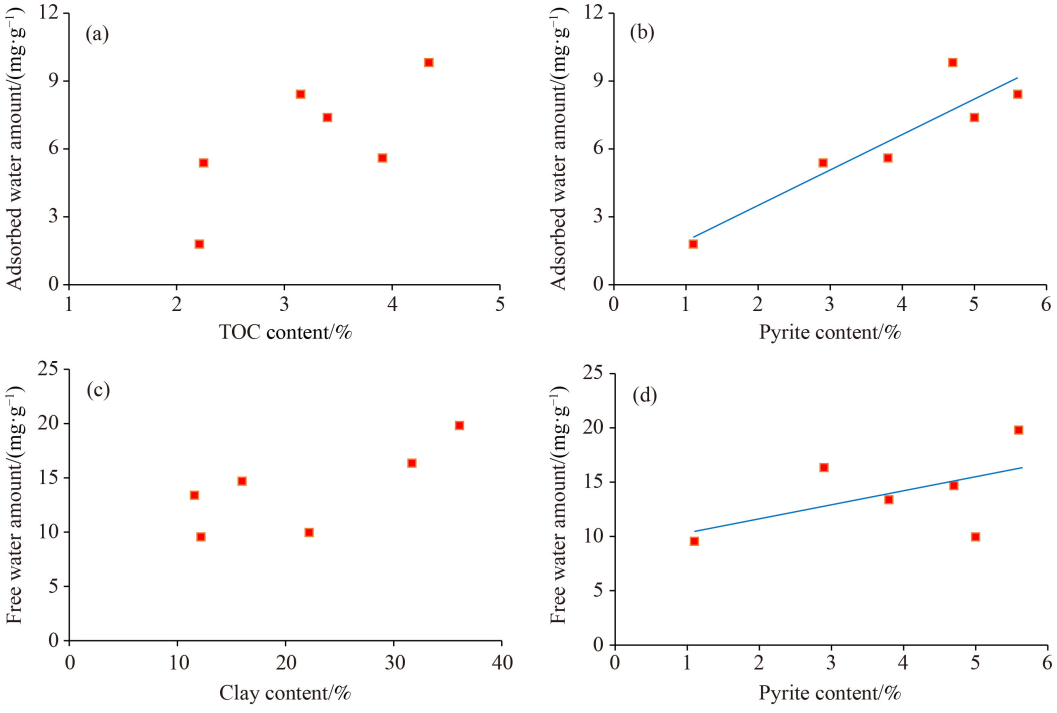


**Fig. 12** Relationship between adsorbed water/free water amounts and material composition.

## References


Ahmad M, Haghighi M (2013). Water Saturation Evaluation of Murteree and Roseneath Shale Gas Reservoirs, Cooper Basin, Australia Using Wire-line Logs. Focused Ion Beam Milling and Scanning Electron Microscopy

Berner R A (1984). Sedimentary pyrite formation: an update. Geochim Cosmochim Acta, 48(4): 605–615

Chalmers G R L, Bustin R M (2007). The organic matter distribution and methane capacity of the lower Cretaceous strata of northeastern British Columbia, Canada. Int J Coal Geol, 70(1–3): 223–239

Chen X, Chen L, Tan X, Jiang S, Wang C (2021). Impact of pyrite on shale gas enrichment—a case study of the lower Silurian Longmaxi Formation in southeast Sichuan Basin. Front Earth Sci, 15(2): 332–342

Cheng P, Tian H, Xiao X, Gai H, Li T, Wang X (2017). Water distribution in overmature organic-rich shales: implications from water adsorption experiments. Energy Fuels, 31(12): 13120–13132

Dehghanpour H, Lan Q, Saeed Y, Fei H, Qi Z (2013). Spontaneous imbibition of brine and oil in gas shales: effect of water adsorption and resulting microfractures. Energy Fuels, 27(6): 3039–3049

Dong D, Shi Z, Guan Q, Jiang S, Zhang M, Zhang C, Wang S, Sun S, Yu R, Liu D, Peng P, Wang S (2018). Progress, challenges and prospects of shale gas exploration in the Wufeng–Longmaxi reservoirs in the Sichuan Basin. Natural Gas Industry B, 5(5): 415–424

Fang C, Huang Z, Wang Q, Zheng D, Liu H (2014). Cause and significance of the ultra-low water saturation in gas-enriched shale reservoir. Nat Gas Geosci, 25(3): 471–476

Gasparik M, Bertier P, Gensterblum Y, Ghanizadeh A, Krooss B M, Littke R (2014). Geological controls on the methane storage capacity in organic-rich shales. Int J Coal Geol, 123: 34–51

Guo X, Hu D, Li Y, Wei Z, Wei X, Liu Z (2017). Geological factors controlling shale gas enrichment and high production in Fuling shale gas field. Pet Explor Dev, 44(4): 513–523

Hao F, Zou H, Lu Y (2013). Mechanisms of shale gas storage: implications for shale gas exploration in China. AAPG Bull, 97(8): 1325–1346

Hu Y, Devegowda D, Striolo A, Van Phan A T, Ho T A, Civan F, Sigal R (2015). Microscopic dynamics of water and hydrocarbon in shale-kerogen pores of potentially mixed wettability. SPE J, 20(01): 112–124

Jiang L, Sun H, Yang S, Zhang Y, Xu H (2020). Investigation on multi-scale pore seepage model of shale gas reservoir considering diffusion and slippage effect. Microfluid Nanofluidics, 24(11): 83

Jiang T, Bian X, Wang H, Li S, Jia C, Liu H, Sun H (2017). Volume fracturing of deep shale gas horizontal wells. Nat Gas Ind B, 4(2): 127–133

Jiao F (2019). Theoretical insights, core technologies and practices concerning “volume development” of shale gas in China. Nat Gas Ind B, 6(6): 525–538

Jin Z, Nie H, Liu Q, Zhao J, Jiang T (2018). Source and seal coupling mechanism for shale gas enrichment in upper Ordovician Wufeng Formation – lower Silurian Longmaxi Formation in Sichuan Basin and its periphery. Mar Pet Geol, 97: 78–93

Larsen J W, Aida M T (2004). Kerogen chemistry 1. Sorption of water by Type II kerogens at room temperature. Energy Fuels, 18(5): 1603–1604

Li J, Li X, Wang X, Li Y, Wu K, Shi J, Yang L, Feng D, Zhang T, Yu P (2016). Water distribution characteristic and effect on methane adsorption capacity in shale clay. Int J Coal Geol, 159: 135–154

Li J, Li X, Wu K, Feng D, Zhang T, Zhang Y (2017a). Thickness and stability of water film confined inside nanoslits and nanocapillaries of shale and clay. Int J Coal Geol, 179: 253–268

Li J, Lu S, Cai J, Zhang P, Xue H, Zhao X (2018). Adsorbed and free oil in lacustrine nanoporous shale: a theoretical model and a case study. Energy Fuels, 32(12): 12247–12258

Li J, Lu S, Xie L, Zhang J, Xue H, Zhang P, Tian S (2017b). Modeling of hydrocarbon adsorption on continental oil shale: a case study on *n*-alkane. Fuel, 206: 603–613

Li J, Wang S, Lu S, Zhang P, Cai J, Zhao J, Li W (2019a). Microdistribution and mobility of water in gas shale: a theoretical and experimental study. Mar Pet Geol, 102: 496–507

Li R, Wu K, Li J, Xu J, Chen Z (2019b). Shale gas transport in wedged nanopores with water films. J Nat Gas Sci Eng, 66: 217–232

Liang C, Jiang Z, Zhang C, Guo L, Yang Y, Li J (2014). The shale characteristics and shale gas exploration prospects of the lower Silurian Longmaxi Shale, Sichuan Basin, south China. J Nat Gas Sci Eng, 21: 636–648

Long S, Feng D, Li F, Du W (2018). Prospect analysis of the deep marine shale gas exploration and development in the Sichuan Basin, China. J Nat Gas Geosci, 3(4): 181–189

Loucks R G, Reed R M, Ruppel S C, Jarvie D M (2009). Morphology, genesis, and distribution of nanometer-scale pores in siliceous mudstones of the Mississippian Barnett Shale. J Sediment Res, 79(12): 848–861

Ma X, Li X, Liang F, Wan Y, Shi Q, Wang Y, Zhang X, Che M, Guo W, Guo W (2020). Dominating factors on well productivity and development strategies optimization in Weiyuan shale gas play, Sichuan Basin, SW China. Pet Explor Dev, 47(3): 594–602

Odusina E, Sondergeld C, Rai C (2011). An NMR study on shale wettability. SPE: Calgary, Alberta, Canada; SPE-147371-MS

Pan Z, Connell L D, Camilleri M, Connelly L (2010). Effects of matrix moisture on gas diffusion and flow in coal. Fuel, 89(11): 3207–3217

Ross D J K, Marc Bustin R (2009). The importance of shale composition and pore structure upon gas storage potential of shale Gas Reservoirs. Mar Pet Geol, 26(6): 916–927

Sang G, Liu S, Elsworth D, Yang Y, Fan L (2020). Evaluation and modeling of water vapor sorption and transport in nanoporous shale. Int J Coal Geol, 228: 103553

Sang G, Liu S, Zhang R, Elsworth D, He L (2018). Nanopore characterization of mine roof shales by SANS, nitrogen adsorption, and mercury intrusion: impact on water adsorption/retention behavior. Int J Coal Geol, 200: 173–185

Sheng G, Su Y, Zhao H, Liu J (2020). A unified apparent porosity/permeability model of organic porous media: coupling complex pore structure and multi-migration mechanism. Adv Geo-Energy Res, 4(2): 115–125

Tang X, Ripepi N, Valentine K A, Keles C, Long T, Gonciaruk A

(2017). Water vapor sorption on Marcellus shale: measurement, modeling and thermodynamic analysis. Fuel, 209(1): 606–614

Tian H, Wang M, Liu S, Zhang S, Zou C (2020). Influence of pore water on the gas storage of organic-rich shale. Energy Fuels, 34(5): 5293–5306

Wang P, Li X (2006). Thermal-weightlessness method to determine water content and existing form of hydratable clay. Nat Gas Ind, 26(1): 80–83

Wang T, Tian S, Li G, Sheng M, Ren W, Liu Q, Tan Y, Zhang P (2019). Experimental study of water vapor adsorption behaviors on shale. Fuel, 248: 168–177

Wu K, Chen Z, Li X, Guo C, Wei M (2016). A Model for multiple transport mechanisms through nanopores of shale gas reservoirs with real gas effect–adsorption-mechanic coupling. Int J Heat Mass Transf, 93: 408–426

Wu Q, Bai B, Ma Y, Ok J T, Neeves K B, Yin X (2014). Optic imaging of two-phase-flow behavior in 1D nanoscale channels. SPE J, 19(5): 793–802

Xie L, Lu S, Li J, Hu Y, Zhang P, Chen J, Zhang P (2015). Experimental investigations of the mineral wettability in shale and its influence factors. Acta Geol Sin, 89(s1): 170–171

Xu L, Wei H, Chen L, Liu L, Jiang Z, Yang K, Li X (2022). Storing characteristics and main controlling factors of connate water in lower Paleozoic Shales in Southeast Chongqing, China. J Petrol Sci Eng, 215: 110543

Yang B, Kang Y, You L, Li X, Chen Q (2016). Measurement of the surface diffusion coefficient for adsorbed gas in the fine mesopores and micropores of shale organic matter. Fuel, 181: 793–804

Yang R, Jia A, He S, Hu Q, Sun M, Dong T, Hou Y, Zhou S (2021). Experimental investigation of water vapor adsorption isotherm on gas-producing Longmaxi Shale: mathematical modeling and implication for water distribution in shale reservoirs. Chem Eng J, 406: 125982

Yang R, Jia A, Hu Q, Guo X, Sun M (2020). Particle size effect on water vapor sorption measurement of organic shale: one example from Dongyuemiao Member of lower Jurassic Ziliujing Formation in Jiannan area of China. Adv Geo-Energy Res, 4(2): 207–218

Yi J, Bao H, Zheng A, Zhang B, Shu Z, Li J, Wang C (2019). Main factors controlling marine shale gas enrichment and high-yield wells in South China: a case study of the Fuling shale gas field. Mar Pet Geol, 103: 114–125

Yuan W, Pan Z, Li X, Yang Y, Zhao C, Connell L D, Li S, He J (2014). Experimental study and modelling of methane adsorption and diffusion in shale. Fuel, 117: 509–519

Yuan Y, Rezaee R, Verrall M, Hu S Y, Zou J, Testmanti N (2018). Pore characterization and clay bound water assessment in shale with a combination of NMR and low-pressure nitrogen gas adsorption. Int J Coal Geol, 194: 11–21

Zhang J, Shi M, Wang D, Tong Z, Hou X, Niu J, Li X, Li Z, Zhang P, Huang Y (2022). Fields and directions for shale gas exploration in China. Nat Gas Ind B, 9(1): 20–32

Zhang T, Li X, Sun Z, Feng D, Miao Y, Li P, Zhang Z (2017). An analytical model for relative permeability in water-wet nanoporous media. Chem Eng Sci, 174: 1–12

Zhu Y, Chen G, Liu Y, Shi X, Wu W, Luo C, Yang X, Yang Y, Zou Y (2021). Sequence stratigraphy and lithofacies paleogeographic evolution of Katian Stage – Aeronian Stage in southern Sichuan Basin, SW China. Pet Explor Dev, 48(5): 1126–1138

Zou C, Dong D, Wang Y, Li X, Huang J, Wang S, Guan Q, Zhang C, Wang H, Liu H, Bai W, Liang F, Lin W, Zhao Q, Liu D, Yang Z, Liang P, Sun S, Qiu Z (2016). Shale gas in China: characteristics, challenges and prospects (II). Pet Explor Dev, 43(2): 182–196